Understanding Device-Structure-Induced Variations in Open-Circuit Voltage for Organic Photovoltaics

ARTICLE *in* ACS APPLIED MATERIALS & INTERFACES · MAY 2015

Impact Factor: 6.72 · DOI: 10.1021/acsami.5b01723 · Source: PubMed

7 AUTHORS, INCLUDING:

Zhiping Wang

National Institute of Advanced Industrial Scie…

10 PUBLICATIONS **59** CITATIONS

SEE PROFILE

Ying Zhou

National Institute of Advanced Industrial Scie…

23 PUBLICATIONS **216** CITATIONS

SEE PROFILE

Yuji Yoshida

National Institute of Advanced Industrial Scie…

121 PUBLICATIONS **1,840** CITATIONS

SEE PROFILE

Masayuki Chikamatsu

National Institute of Advanced Industrial Scie…

60 PUBLICATIONS **786** CITATIONS

SEE PROFILE

ACS APPLIED MATERIALS & INTERFACES

Research Article

www.acsami.org

Understanding Device-Structure-Induced Variations in Open-Circuit Voltage for Organic Photovoltaics

Zhiping Wang,*[,†] Yu Uemura,[‡] Ying Zhou,[§] Tetsuhiko Miyadera,[†,∥] Reiko Azumi,[§] Yuji Yoshida,[†] and Masayuki Chikamatsu[†]

[†]Research Center for Photovoltaic Technologies and [§]Electronics and Photonics Research Institute,National Institute of Advanced Industrial Science and Technology (AIST), AIST Tsukuba Central 5, 1-1-1 Higashi, 305-8565 Tsukuba, Japan

[‡]Faculty of Engineering, Department of Nanoscience, Sojo University, 4-22-1 Ikeda, Nishi-ku, Kumamoto 860-0082, Japan

[∥]Japan Science and Technology Agency (JST)-PRESTO, 4-1-8 Honcho Kawaguchi, 332-0012 Saitama, Japan

Supporting Information

ABSTRACT: We investigate the structural influences on the device performance, especially on open-circuit voltage (V_{OC}) in squaraine (SQ)/fullerene (C_{60}) bilayer cells. Simply changing the SQ thickness could lead to 40% variation in V_{OC} from 0.62 to 0.86 V. The ionization potential (IP) of SQ films and recombination at the anode surface as well as donor/acceptor (D/A) interface sensitively vary with film thicknesses, which account for the shifts in V_{OC}. The anode recombination can be effectively suppressed by preventing direct contact between C_{60} and the anode with a buffer layer, delivering an elevated V_{OC}. Through polarized infrared−multiple-angle incidence resolution spectroscopy measurement, the molecular structure of SQ films is found to gradually evolve from lying-down on indium−tin oxide substrates with noncentrosymmetric orientation at low thicknesses to random structure at high thicknesses. The different molecular orientation may yield different strengths of electronic coupling, which affects the charge-carrier recombination and thus V_{OC}. Moreover, the oriented SQ films would spontaneously compose aligned dipole moments at the D/A interface because of the strong dipolar effects in SQ molecules identified by density functional theory calculations, whereas no aligned interfacial dipole moment exists in the random structure. The resulting interfacial dipole moments would form an electric field at the D/A interface, leading to variations in the IP and thus impacting V_{OC}. Our findings demonstrate that V_{OC} in organic photovoltaic cells is critically associated with the molecular orientation that affects the charge-carrier recombination and interfacial dipole alignment, which should be seriously taken into consideration for the design of organic molecules and optimization of the cell efficiency.

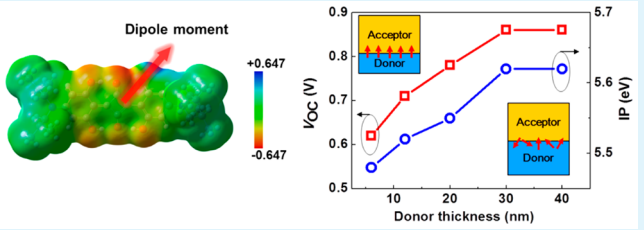

KEYWORDS: *open-circuit voltage, structural control, molecular orientation, organic photovoltaics*

INTRODUCTION

Organic photovoltaic (OPV) cells are some of the most competitive candidates for solar-energy conversion applications because of their potential for low-cost production and advantages such as light weight, flexibility, and solution processability.[1−5] The power conversion efficiency (PCE) of OPV single-junction cells has been steadily improved because of the development of new materials and device architectures, reaching 8.9% in a small-molecule cell[6] and 9.2% in a polymer-based cell.[7] Recently, tandem OPV cells have been reported to reach a PCE of 11.3% and 11.5% based on small molecules[8] and polymers,[9] respectively. In order to further boost PCE for commercialization, tremendous efforts have been made to improve solar cell characteristics, including the short-circuit current (J_{SC}), fill factor (FF), and open-circuit voltage (V_{OC}). Structural control featuring regulation of the crystallinity, molecular orientation, and morphology is one of the most effective strategies to improving J_{SC} and FF.[10,11] Our recent studies demonstrated that tailoring the nanostructure of organic films at the molecular level leads to lying-down molecular geometry, phase-separated morphology in coevaporated blend films, and increased charge-carrier lifetime, which have substantially improved J_{SC} and FF.[12−15] Meanwhile, we found that many devices more or less show unstable V_{OC} shifting with the structural properties such as the film thickness, molecular orientation, etc. However, a systematic discussion with respect to the structure−V_{OC} relationship remains scarce.

Achieving high V_{OC} has long been recognized as a vital challenge for molecular-based solar cells. V_{OC} depends on the interfacial energy level offset (ΔE_{DA}) between the highest occupied molecular orbital (HOMO) energy levels of donor materials and the lowest unoccupied molecular orbital (LUMO) energy levels of acceptor materials,[16−18] as well as charge separation/recombination kinetics.[19] Until now, ap-

Received: February 24, 2015
Accepted: May 6, 2015
Published: May 6, 2015

DOI: 10.1021/acsami.5b01723
ACS Appl. Mater. Interfaces 2015, 7, 10814−10822

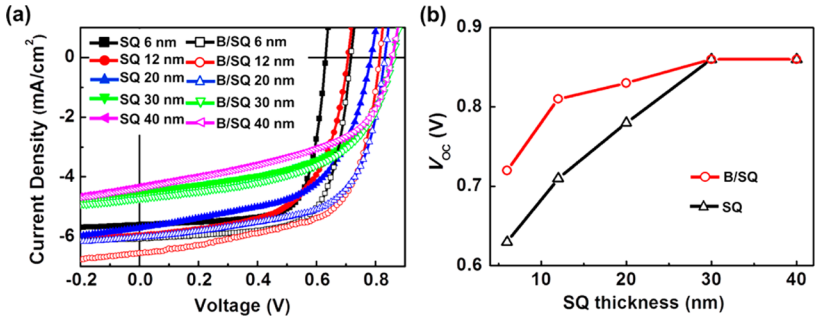

Figure 1. (a) Current density versus voltage (J–V) characteristics of OPV cells with structures of ITO/BP2T (0 or 8 nm)/SQ (6–40 nm)/C_{60} (40 nm)/BCP (3 nm)/Al (100 nm). (b) V_{OC} as a function of the SQ thickness extracted from part a. B/SQ stands for BP2T/SQ.

proaches for the development of V_{OC} can be briefly summarized as (1) extending ΔE_{DA} by lifting the LUMO of the acceptor and/or by shifting down the HOMO of the donor by molecular design[20−24] and (2) minimizing the charge-carrier recombination by controlling the morphology,[25] introducing buffer layers,[26] etc. Considerable studies have been focused on the first approach by developing various donor materials with low HOMO levels, such as 2,4-bis[4-(*N*,*N*-diisobutylamino)-2,6-dihydroxyphenyl]squaraine (SQ),[17] tetraphenyldibenzoperiflanthen,[18] and poly[*N*-9′-heptadecanyl-2,7-carbazole-*alt*-5,5-(4′,7′-di-2-thienyl-2′,1′,3′-benzothiadiazole)],[19] and/or by developing acceptor materials with high LUMO levels, such as an indene-C_{60} bisadduct.[20] For OPV cells with a certain donor/acceptor (D/A) material system, V_{OC} is sometimes observed to shift with the cell parameters, such as the blending ratio, film thicknesses, and buffer layers,[27−31] which largely affects the ultimate cell efficiencies. For some organic molecules that have been well-studied, such as zinc phthalocyanine, nearly changeless V_{OC} has been observed in the OPV cells with different film thicknesses.[32−34] Comparatively, for many advanced organic molecules having deep HOMO levels, the film thickness is seen to have a remarkable impact on V_{OC}.[29,35−37] This implies that thickness control can be crucial for some unique molecules, and investigation on the underlying mechanisms is of great importance for high cell efficiencies.

Previous studies suggest that, despite the same organic material, multiple electronic structures are found for films with different thicknesses because of variations in the molecular orientation.[38−40] The structural order at the D/A interface of planar heterojunctions can also be a crucial factor that affects the electronic coupling and thus the recombination rate.[41,42] On the other hand, Duhm et al. demonstrated that the ionization potential (IP) of organic films depends strongly on the orientation of the molecules because of variations in the interfacial dipole moment.[43] Tajima et al. reported that introducing interfacial dipole moments at the D/A interface allows the relative energy levels of the materials to be tuned.[19,44] On the basis of the observations mentioned above, V_{OC} can be affected by structural properties such as the electronic coupling of materials and interfacial dipole moments induced by the molecular orientation. A thorough understanding of the correlation between the molecular orientation and V_{OC} is highly required for maximization of the potential of materials and for further improvement of the OPV cells.

In the present work, we investigate the influence of the device structure on V_{OC} in SQ/fullerene (C_{60}) planar heterojunction OPV cells by employing SQ layers with different thicknesses. The OPV cells suffer from serious surface recombination between indium–tin oxide (ITO) anode and C_{60} by virtue of the discontinuous SQ morphology at low thicknesses, resulting in low V_{OC}. With the introduction of a 2,5-bis(4-biphenylyl)bithiophene (BP2T) layer on ITO, this recombination-induced V_{OC} loss could be substantially suppressed. Variation in ΔE_{DA} is found to be another important reason for the changes in V_{OC} via analysis of the temperature dependence of cell characteristics and photoemission spectra. Polarized infrared–multiple-angle incidence resolution spectroscopy (FTIR–MAIRS) measurement reveals that the SQ films are noncentrosymmetrically oriented on ITO substrates at low thicknesses but gradually evolve into a random structure as the film thickness increases. The molecular orientation may affect the strength of the electronic coupling at the D/A interface and thus the charge-carrier recombination, which is also responsible for variations in V_{OC}. Furthermore, on the basis of density functional theory (DFT) calculations, the oriented SQ films would spontaneously form a layer of aligned dipole moments at the D/A interface, which affects the IP of the SQ films and, in turn, influences V_{OC}.

EXPERIMENTAL SECTION

OPV Cell Fabrication. All photovoltaic cells were fabricated on commercially available ITO-coated glass substrates that were pretreated in oxygen plasma for 30 min. Prior to use, BP2T (Aldrich) was further purified three times by vacuum gradient sublimation, and SQ (Aldrich) was purified twice by column chromatography on silica gel with chloroform as the eluent and recrystallized from chloroform/hexane. C_{60} (Frontier Carbon, 99.9%) and bathocuproine (BCP; Dojindo, 98%) were used as received. These materials were thermally evaporated in a vacuum chamber ($<2 \times 10^{-5}$ Pa) at room temperature with the following rates: BP2T, 0.10 ± 0.05 Å/s; SQ, 0.10 ± 0.05 Å/s; C_{60}, 0.10 ± 0.05 Å/s; BCP, 0.35 ± 0.05 Å/s; Al, 1.5 ± 0.5 Å/s. All film thicknesses and deposition rates were monitored using a quartz crystal oscillator. Cells were fabricated with a simple p–n heterojunction architecture ITO/buffer layer (BP2T: 0 or 8 nm)/donor (SQ: 6, 12, 20, 30, or 40 nm)/acceptor (C_{60}: 40 nm)/BCP (3 nm)/Al (100 nm). More than eight separate cells were fabricated under each condition to estimate the variability.

Characterizations and Theoretical Calculations. The current density versus voltage (J–V) characteristics of the cells were measured under dark conditions and simulated solar illumination (AM 1.5G) using a digital source meter (Keithley 2400). The incident power was calibrated using a standard calibrated silicon cell to match 1-sun intensity (100 mW/cm^2). For low-temperature measurement, the OPV cells were characterized in a vacuum chamber ($<5 \times 10^{-4}$ Pa). All of the cells were mounted into the vacuum chamber through a glovebox without exposure to the ambient environment. The cell temperature was varied in a range between 125 and 300 K using a liquid-nitrogen cooling system and a cryostat. The IP levels of the SQ and BP2T/SQ films were determined by photoelectron yield

DOI: 10.1021/acsami.5b01723
ACS Appl. Mater. Interfaces 2015, 7, 10814–10822

Table 1. Cell Performances of ITO/BP2T (0 or 8 nm)/SQ (6−40 nm)/C_{60} (40 nm)/BCP (3 nm)/Al (100 nm) under 1 sun Illumination together with the Saturation Current, Ideality Factor, and Calculated Slope Values

cell	PCE [%]	J_{SC} [mA/cm^2]	V_{OC} [V]	FF	J_{SO}[mA/cm^2]	n^a	calculated slope^b
SQ 6 nm	2.5 ± 0.2	5.6 ± 0.2	0.62 ± 0.01	0.71 ± 0.02	1.6×10^{-3}	1.87	-1.3×10^{-3}
SQ 12 nm	2.6 ± 0.2	5.9 ± 0.2	0.71 ± 0.01	0.61 ± 0.02	9.4×10^{-4}	1.50	-1.1×10^{-3}
SQ 20 nm	2.5 ± 0.2	5.7 ± 0.2	0.78 ± 0.01	0.56 ± 0.02	6.9×10^{-4}	1.27	-9.9×10^{-4}
SQ 30 nm	2.0 ± 0.1	4.5 ± 0.1	0.86 ± 0.01	0.53 ± 0.02	3.2×10^{-4}	1.16	-9.5×10^{-4}
SQ 40 nm	1.6 ± 0.1	4.3 ± 0.1	0.86 ± 0.01	0.43 ± 0.02	2.8×10^{-4}	1.15	-9.5×10^{-4}
BP2T/SQ 6 nm	3.0 ± 0.2	6.0 ± 0.2	0.72 ± 0.01	0.70 ± 0.02	8.9×10^{-4}	1.55	-1.2×10^{-3}
BP2T/SQ 12 nm	3.3 ± 0.2	6.5 ± 0.2	0.81 ± 0.01	0.63 ± 0.02	4.5×10^{-4}	1.20	-9.9×10^{-4}
BP2T/SQ 20 nm	3.1 ± 0.2	6.0 ± 0.1	0.83 ± 0.01	0.63 ± 0.02	4.2×10^{-4}	1.20	-9.9×10^{-4}
BP2T/SQ 30 nm	2.1 ± 0.1	4.7 ± 0.1	0.86 ± 0.01	0.53 ± 0.02	3.1×10^{-4}	1.15	-9.5×10^{-4}
BP2T/SQ 40 nm	1.7 ± 0.1	4.3 ± 0.1	0.86 ± 0.01	0.44 ± 0.02	2.9×10^{-4}	1.15	-9.5×10^{-4}

$^a n$ is calculated according to eq 1 using the ΔE_{DA} values estimated from the IP. ^{b}The calculated slope values are obtained from $-nkq^{-1} \ln(J_{SC}/J_{SO})$.

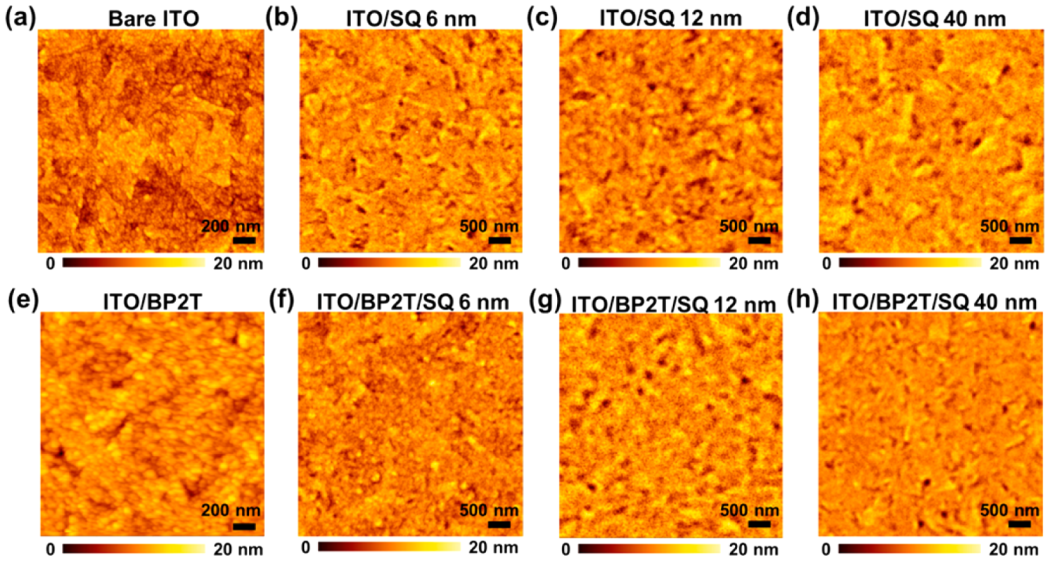

Figure 2. AFM height images of (a) bare ITO, (b) ITO/SQ (6 nm), (c) ITO/SQ (12 nm), (d) ITO/SQ (40 nm), (e) ITO/BP2T, (f) ITO/BP2T/SQ (6 nm), (g) ITO/BP2T/SQ (12 nm), and (h) ITO/BP2T/SQ (40 nm). The thickness of the BP2T layer is 8 nm. The rms roughness of parts a−h are 2.3, 1.8, 1.7, 1.6, 1.9, 1.6, 1.7, and 1.7 nm, respectively.

spectroscopy (PYS; Bunkoukeiki BIP-KV200) in a vacuum chamber (<5 × 10^{-3} Pa). Note that all of the films for IP measurement were deposited on the ITO substrate and were subsequently transferred into the vacuum chamber under a N_2 atmosphere. Grazing incidence wide-angle X-ray scattering (GIWAXS) experiments were performed at Spring-8 (beamline BL46XU; beam energy = 10.3 keV) in Hyogo, Japan. For FTIR−MAIRS measurements, pure SQ films with different thicknesses were deposited on CaF_2 substrates. The FTIR−MAIRS spectra were measured using a FTIR spectroscopy (FTIR-6000, JASCO, Japan) equipped with a MAIRS automatic measurement unit (AM-4000). Absorption spectra were collected using an ultraviolet−visible−near-infrared (UV−vis−NIR) spectrophotometer (Shimadzu UV-3600). For the above-mentioned material characterizations, all of the SQ samples were prepared using the same procedure as that used for fabricating OPV cells. The molecular geometry optimizations and vibrational frequency calculations were performed with the *Gaussian 09* software package using a DFT approach. Becke's three-parameter hybrid functional with the LYP correlation functional (B3LYP) was employed together with the 6-31G(d) basis set. The dipole moment of the molecule was performed by Mulliken population analysis based on DFT calculations. The electrostatic potential (ESP) of the molecule was mapped on the van der Waals surface.

RESULTS AND DISCUSSION

The $J-V$ characteristics of BP2T (0 or 8 nm)/SQ/C_{60} OPV cells with different SQ thicknesses under 1 sun illumination are presented in Figure 1a and Table 1. For the OPV cells without BP2T, J_{SC} slightly increases with the SQ thickness at first and then decreases drastically after it reaches the highest value of 5.9 ± 0.2 mA/cm^2 at 12 nm. FF drops continuously with increasing thickness. Comparatively, V_{OC} is found to shift dramatically with different thicknesses. The D/A interface morphology may be one reason that affects the cell characteristics. Figure 2 shows the atomic force microscopy (AFM) images of SQ films with different thicknesses. However, all of the SQ films display similar morphology and root-mean-square (rms) roughness, which is indicative of its negligible impact on the cell characteristics. It is speculated that when the thickness is less than 12 nm, most of photogenerated excitons are able to diffuse to the D/A interface, where they can be efficiently dissociated into free charges. Therefore, J_{SC} is seen to increase along with the thickness below 12 nm. In contrast, at higher thicknesses (over 12 nm) that exceed the exciton diffusion length (L_D), the amount of dissociable excitons no longer increases; instead, the bulk resistance would become larger, resulting in decreased J_{SC} and FF. It is worth mentioning that L_D of the SQ films has been reported to be around 5 nm,[45] which is shorter than the L_D value (12 nm) observed in our case. We assume that when a very thin SQ film is deposited on the ITO substrate, a discontinuous film may be formed because

DOI: 10.1021/acsami.5b01723
ACS Appl. Mater. Interfaces 2015, 7, 10814−10822

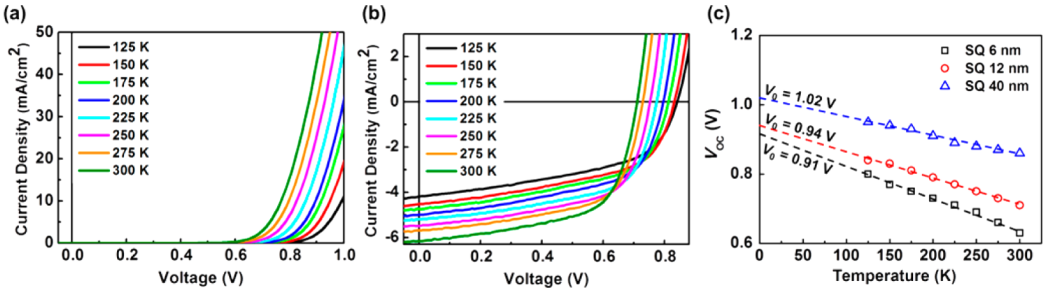

Figure 3. $J-V$ characteristics of an ITO/SQ (12 nm)/C_{60} (40 nm)/BCP (3 nm)/Al (100 nm) structured cell in the dark (a) and in 1 sun illumination (b) under various temperatures ranging from 125 to 300 K, (c) V_{OC} as a function of the temperature extracted from the temperature-dependent measurement of OPV cells with 6, 12, and 40 nm SQ films. All of the measured data points are fitted linearly (dashed line) to extrapolate the interfacial energy offset ΔE_{DA} (i.e., V_0) according to eq 1. The slope of the fitting lines for SQ 6, 12, and 40 nm are -9.1×10^{-4}, -7.7×10^{-4}, and -5.5×10^{-4}, respectively.

of the rough ITO surface (rms value, 2.3 nm; Figure 2a). Therefore, a dispersed rather than a perfectly flat D/A interface is more likely to be formed in the actual cell, which enables efficient exciton dissociation despite a short L_D. On the other hand, V_{OC} exhibits only 0.62 V for OPV cells with 6 nm SQ films, while it gradually increases with the SQ thickness and finally saturates to a certain value of 0.86 V (Figure 1b). The discontinuous SQ films at low thicknesses would lead to direct contact between C_{60} and the ITO anode, forming a Schottky junction,[46] which can be one of the reasons for the low V_{OC} value. To reduce the uncertainty induced by such a Schottky contact, an 8 nm layer of the wide-band-gap material BP2T is inserted between the ITO and SQ films, serving not only as a contact-preventing layer but also as a hole-transporting and electron-blocking layer because of its suitable energy alignment with SQ (Figure S1 in the Supporting Information, SI). The introduction of BP2T has substantially improved J_{SC} and V_{OC} at low SQ thicknesses (below 20 nm); however, it has less effect at high SQ thicknesses (30 and 40 nm) because ITO and C_{60} no longer have contact with each other. Additionally, because BP2T films absorb photons from 300−500 nm (Figure S2 in the SI), generating excitons, cascade-type devices can be formed by introducing BP2T. Such a cascade structure may drive efficient exciton transfer from the anode to the dissociating SQ/C_{60} interface,[13] which is attributed to the photocurrent. This can be another reason for the improved J_{SC} value of OPV cells with BP2T. Despite the improvement, V_{OC} of the OPV cells with the BP2T layer remains of thickness similar to that of the OPV cells without BP2T (Figure 1b). It is believed that the SQ films at low thicknesses still exhibit discontinuous morphology on BP2T, which results in direct contact between C_{60} and BP2T. Because the charge-carrier mobility in the BP2T film is higher than that in the SQ film,[15] the C_{60}/BP2T contact would serve as an additional shunt pathway for charge-carrier transport, which can be responsible for reduced V_{OC} at low film thickness.[47]

In actual cells, many factors may affect V_{OC}, including the IP of donor materials, electron affinity of acceptor materials, various recombination processes, etc.[48] According to an equivalent circuit model based on a diode and a current source modeling the photocurrent,[49−52] V_{OC} can be expressed as

$$V_{OC} = \frac{\Delta E_{DA}}{q} - \frac{nkT}{q} \ln\left(\frac{J_{SC}}{J_{SO}}\right) \quad (1)$$

where n is the ideality factor, k is the Boltzmann constant, T is the temperature, q is the elementary charge, and J_{SO} is the saturation current density. J_{SO} represents the current density of minority carriers, which is a summation of the hole current in the acceptor and the electron current in the donor that are thermally generated at the D/A interface or within the film bulk. As shown in Table 1, J_{SO} decreases with increasing SQ thickness. The magnitude of J_{SO} depends on a number of material properties that determine the charge-carrier recombination kinetics,[53] being independent of ΔE_{DA}. The decreased J_{SO} implies reduced recombination in the OPV cells, resulting in the enhanced V_{OC}. The introduction of BP2T decreases J_{SO} at low thicknesses, while it hardly influences J_{SO} at high thicknesses. This result is in accordance with the previous prediction of the suppressed surface recombination with BP2T buffer layers.

The $J-V$ characteristics of the OPV cells are measured for a range of temperatures from 125 to 300 K under 1 sun illumination. All of the measured OPV cells exhibit analogous temperature dependence, as shown in Figure 3a,b and S3 in the SI. V_{OC} increases steadily with decreasing temperature, while J_{SC} and FF change reversely. Similar phenomena have also been observed for other material systems.[54−56] Reduced L_D[57] and declined charge-carrier mobility[58] at low temperatures account for the continuous decrease in J_{SC}. Additionally, the decreased charge-carrier mobility also gives a high charge-carrier density in the bulk films, which would increase the nongeminate recombination rate,[52] resulting in a reduced charge extraction efficiency. Therefore, decreases in the FF are observed at low temperature. The continuous increase in V_{OC} with decreasing temperature is mainly driven by a corresponding reduction in the dark current (Figure 3a).[56] The temperature dependence of V_{OC} in the OPV cells with different SQ thicknesses is further plotted and fitted in Figure 3c. V_{OC} is linearly dependent upon the temperature with a negative slope, which is consistent with eq 1. The slopes of the fitting lines for SQ 6, 12, and 40 nm are -9.1×10^{-4}, -7.7×10^{-4}, and -5.5×10^{-4}, respectively, which are close to the slope values calculated based on eq 1, as shown in Table 1. Because the slope is equal to $-nkq^{-1} \ln(J_{SC}/J_{SO})$, an OPV cell having a higher recombination rate (i.e., larger n and J_{SO}) would exhibit a steeper increase of V_{OC} with decreasing temperature. Accordingly, the increased slope value with the SQ thickness, in turn, reveals a reduced recombination rate in the OPV cells. With the introduction of BP2T, the OPV cell also shows an elevated slope value (lower recombination rate), as shown in Figure S4 in the SI. These results show coherent conclusion with the aforementioned observation. On the other hand, according to eq 1, by decreasing the temperature T, V_{OC} at $T \sim 0$ K (V_0) approaches $\Delta E_{DA}/q$. Thus, ΔE_{DA} can be

DOI: 10.1021/acsami.5b01723
ACS Appl. Mater. Interfaces 2015, 7, 10814−10822

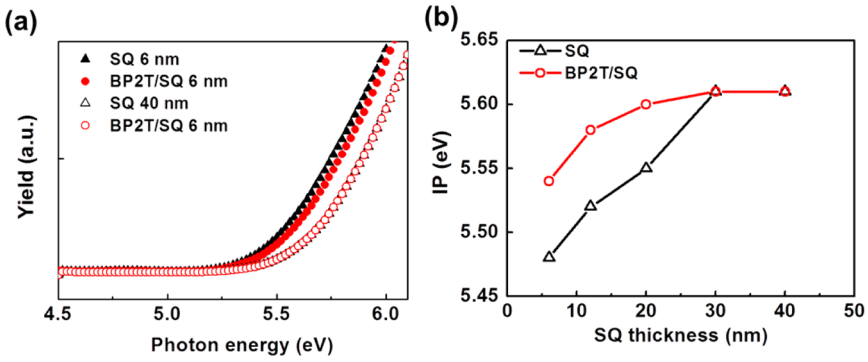

Figure 4. (a) Photoemission spectra of SQ and BP2T (8 nm)/SQ films with different SQ thicknesses. (b) Plotted IP values as a function of the SQ thickness extracted from the photoemission spectra.

roughly estimated by extrapolating V_0 from a linear fitting of the temperature dependence of V_{OC}, as shown in Figure 3c. Previous studies[50,53] suggest that, for a certain D/A system, V_0 should be the same or very close because of the same ΔE_{DA}. However, the estimated V_0 value in our case increases with the thickness, which is indicative of an increased ΔE_{DA} at the SQ/C_{60} interface. Furthermore, increased V_0 is also observed with the incorporation of BP2T (Figure S4 in the SI). It seems that, besides charge-carrier recombination, variation in ΔE_{DA} can be another crucial reason for the thickness-dependent V_{OC}.

Photoemission spectra of the SQ and BP2T/SQ films with different SQ thicknesses are measured by PYS, as shown in Figure 4 and Table 2. Clearly, the IP values shift with different thicknesses (Figure 4b), showing behavior similar to the variation trends in V_{OC} (Figure 1b). This confirms the previous conclusion that variation in ΔE_{DA} is responsible for the shifts in V_{OC}. When the thickness increases from 6 to 40 nm, V_0 shifts +0.11 V from 0.91 to 1.02 V (Figure 2c). According to eq 1 ($V_0 = \Delta E_{DA}/q$), ΔE_{DA} is estimated to shift +0.11 eV. In contrast, as the IP increases from 0.98 eV at 6 nm to 1.12 eV at 40 nm, ΔE_{DA} is estimated to shift +0.14 eV. Likewise, the estimated ΔE_{DA} values from V_0 and IP are compared in Table 2. All of the ΔE_{DA} values calculated from the IP and from V_0 are very close, which quantitatively verifies the observation (variations in ΔE_{DA}) in the temperature-dependent measurement. In addition, using ΔE_{DA} estimated from the IP, the ideality factor (n) can be calculated in terms of eq 1, as shown in Table 1. All of the ideality factors show values between 1 and 2, indicating that localized states in the interfacial band gap participate in the recombination process.[59] It has been well-defined that the closer the ideality factor is to 2, the more dominant the recombination will be in the OPV cells.[60] The decreasing ideality factor with increasing thickness implies a decreased number of trap states, which proves the aforementioned reduced recombination rate with increasing thickness or with BP2T buffer layers. Furthermore, at 6 nm, V_{OC} is only 0.62 V (Figure 1 and Table 1), which is 0.24 V smaller than the saturation value (0.84 V) observed at 40 nm. This 0.24 V V_{OC} loss can be estimated to be 58% originating from variation in ΔE_{DA} because of the −0.14 eV shifted IP. The rest, a 42% V_{OC} loss, can therefore be originate from the recombination process. Analogously, the recombination-induced V_{OC} loss is estimated to be the highest at low thicknesses and gradually decreases with increasing thickness. This result is in accordance with the conclusion deduced from the slope of the fitting line of V_{OC} temperature dependence (Figure 3c).

Table 2. Summary of IP Data Measured for SQ and BP2T (8 nm)/SQ Films with Different SQ Thicknesses Together with the Estimated ΔE_{DA} Value from the IP and V_0 in the Temperature-Dependent Measurement[a]

sample	IP [eV]	estimated ΔE_{DA} from IP [V]	estimated ΔE_{DA} from qV_0 [V]
SQ 6 nm	5.48	0.98	0.91
SQ 12 nm	5.52	1.02	0.94
SQ 20 nm	5.55	1.05	NA
SQ 30 nm	5.62	1.12	NA
SQ 40 nm	5.62	1.12	1.02
BP2T/SQ 6 nm	5.54	1.04	0.96
BP2T/SQ 12 nm	5.58	1.08	1.01
BP2T/SQ 20 nm	5.60	1.10	NA
BP2T/SQ 30 nm	5.62	1.12	NA
BP2T/SQ 40 nm	5.62	1.12	1.03

[a]The LUMO of C_{60} used for the calculation is assumed to be a constant value of 4.5 eV according to the reported literature.[13]

For organic thin films, the kinetics of photoelectrons in molecules can be influenced by their neighboring molecules. Different molecular orientations would induce variations of the electronic structure at the surface,[61,62] i.e., surface dipole moments, which would affect the amount of photoelectrons spilled out of the bulk into vacuum, resulting in multiple IP values.[63−66] To examine the molecular order in our SQ films with different thicknesses, GIWAXS measurements are performed, as shown in Figure S5 in the SI. However, no crystalline phase of the SQ films can be identified, indicating that all of the films are amorphous. This result is in agreement with previous observations that SQ films always display amorphous structure when prepared without annealing or substrate heating treatment.[67]

FTIR−MAIRS measurement[68,69] is performed to characterize the molecular orientation in such amorphous films, as schematically shown in Figure 5a. The measured FTIR−MAIRS data are presented in Figure 5b−f. For the 6 nm SQ film, the spectra are impervious to the angle of incidence θ with s-polarized light (Figure 5b). When detected with p-polarized light (Figure 5c and 5f), the intensity of the band at 1240 cm^{-1} gradually decreases with increasing θ, while the intensity of the neighboring band at 1260 cm^{-1} changes reversely. This change indicates an oriented structure in the 6 nm SQ film. Note that this oriented structure means a noncentrosymmetric stacking of

DOI: 10.1021/acsami.5b01723
ACS Appl. Mater. Interfaces 2015, 7, 10814−10822

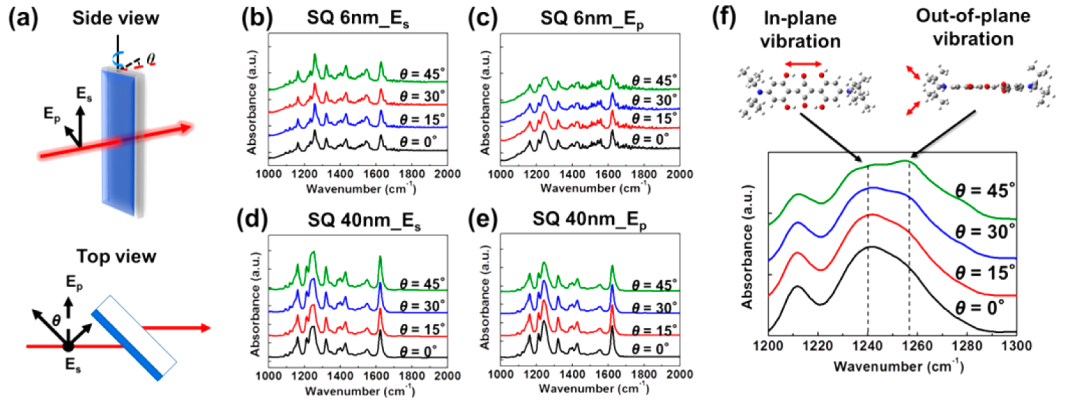

Figure 5. (a) Schematic 3D diagram of the FTIR−MAIRS measurement. FTIR−MAIRS spectra of SQ films: (b) 6 nm with 0° polarization (E_s); (c) 6 nm with 90° polarization (E_p); (d) 40 nm with 0° polarization (E_s); (e) 40 nm with 90° polarization (E_p). (f) Enlarged spectra of part c. In part a, the 0° polarization (E_s; thick circle) is perpendicular to the paper plane, while the 90° polarization (E_p; dotted arrow) is in the plane.

SQ molecules, although no long-range order (i.e., amorphous) structure is identified in GIWAXS. The vibrational spectrum of the SQ molecule is calculated by using the DFT method with the B3LYP/6-31G(d) basis set, as shown in Figure S6 in the SI. The band at around 1240 cm^{-1} is found to be attributed to a pure in-plane C−C vibration mode, while the band at around 1260 cm^{-1} corresponds to a mixture of in-plane and out-of-plane C−N vibration modes (Figure 5f and movies S1−S4 in the SI). The spectra in Figure 5f are also analyzed by Gaussian fitting, as shown in Figure S7 in the SI. Apparently, with increasing θ, i.e., with increasing surface normal (sin θ) detecting strength, a stronger out-of-plane vibration mode is observed, which indicates that the out-of-plane C−N bond is standing-up on the substrate; i.e., the molecules are lying-down on the substrates in the 6 nm SQ film. In the 40 nm SQ film (Figure 5e), the changes at around 1260 cm^{-1} disappear and all of the spectra show a changeless band position with respect to θ, suggesting a random molecular structure. The SQ films grown on the BP2T buffer layer also behave similarly, as shown in Figure S8 in the SI. In general, the orientation of the molecules in mono- and multilayers with respect to the substrate critically depends on the relative strength of the molecule−substrate versus intermolecular interaction.[14] SQ molecules are supposed to have strong interaction with the substrate, which may result in a lying-down molecular orientation at 6 nm. However, as the film grows, molecule−substrate interaction no longer exists, and instead intermolecular interaction between molecules gradually dominates the film growth. Owing to the nonplanar molecular structure, $\pi-\pi$ interaction between SQ molecules should be very weak, and therefore random structures are preferentially formed. As a result, a random structure is observed at high thicknesses. Note that the growth of SQ films on ITO and CaF_2 substrates might be different. Unfortunately, because of the strong peaks originating from ITO and glass, it is very difficult to extract accurate FTIR−MAIRS peak information on SQ films grown on ITO substrates. Obvious changes with different SQ thicknesses have been observed in the IP (Figure 4) and optical absorption (Figure 6, vide infra) measurements. Both of them show consistent conclusion with the FTIR−MAIRS results. Therefore, it is reasonable to believe that the SQ molecules show similar growth patterns on ITO glass and on CaF_2 substrates.

Besides FTIR−MAIRS measurement, the molecular orientation is also analyzed by studying the optical absorption

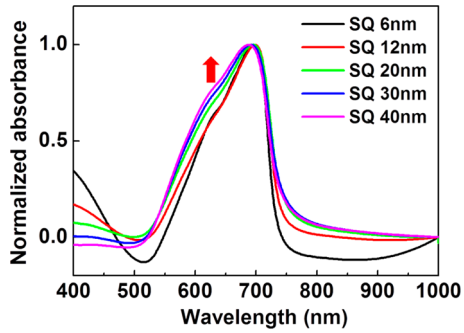

Figure 6. Normalized optical absorption spectra of SQ films on ITO substrates with different SQ thicknesses. The red arrow points out the ascending trend of the intensity of amorphous peak at around 630 nm, indicating a climbing content of the amorphous phase (structural disorder) in the SQ films with increasing thickness.

properties. Figure 6 shows the normalized absorption spectra of SQ films with different thicknesses. The absorption covers a region from 500 to 750 nm. An absorption maximum at around 695 nm and a shoulder peak at around 630 nm can be identified, which are assigned to *J* aggregates and an amorphous monomer, respectively.[70,71] Noticeably, the intensity of the shoulder peak at around 630 nm increases with the thickness, which indicates that the molecular structure changes from head-to-tail (*J*-aggregate) order to a random structure. This result is consistent with the FTIR−MAIRS observation. Moreover, it has been demonstrated that increased structural disorder at the D/A interface reduces the electronic coupling, bringing about decreased recombination rate.[41,42] Accordingly, the random molecular orientation of thick SQ films (larger interfacial disorder compared with that of thin SQ films) would alleviate the recombination at the SQ/C_{60} interface, which can also be responsible for the up-shifted V_{OC}. This result also substantiates the previous conclusion obtained from the temperature-dependent measurement that OPV cells with increasing film thicknesses yield reduced recombination rate (Figure 3).

The dipole moment and ESP of an SQ molecule are calculated using DFT calculations with the B3LYP/6-31G(d) basis set, as shown in Figure 7. The calculated dipole moment is shown as a blue arrow in Figure 7a. The magnitude of the dipole moment is 2.1326 D, composited with a 1.5292 D vector in the *x* axis (long axis of the molecule), a 1.4825 D vector in the *y* axis (short axis of the molecule), and a 0.1099 D vector in

DOI: 10.1021/acsami.5b01723
ACS Appl. Mater. Interfaces 2015, 7, 10814−10822

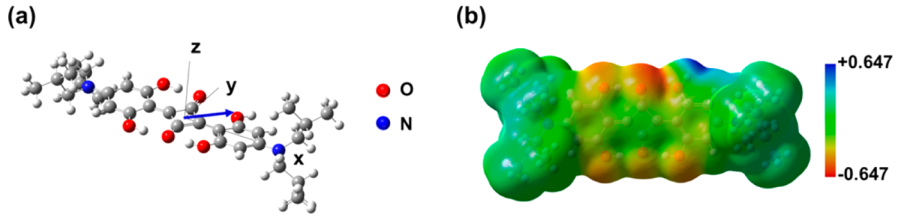

Figure 7. (a) Dipole moment (blue arrow) of a SQ dye and (b) ESP of a SQ dye mapped on the van der Waals surface, obtained with B3LYP/6-31G(d).

the *z* axis (out-of-plane axis of the molecule). The direction of the dipole moment points from the center of the squaraine ring to nearly a half angle of the *x*- and *y*-axis directions. When SQ films are oriented, the topmost-aligned dipolar molecules would spontaneously form intrinsic dipole moments pointing away from the core of the SQ molecule at the surface, which critically affect the IP. ESP of the SQ molecule is mapped on the van der Waals surface, as shown in Figure 7b. An extended region of the lowest ESP (red color) above the oxygen atoms in the SQ ring is observed, while an extended region of much higher ESP (green color) is seen over the nitrogen-terminated ends. It implies that less work is required to promote one electron out of the HOMO to the vacuum region above the oxygen atoms (along the *y*-axis direction) compared with that above the nitrogen-terminated ends (along the *x*-axis direction). When the SQ molecules are preferentially lying-down on the substrates, a high density of oxygen atoms (i.e., surface dipole) would be exposed to the vacuum, forming an electric field at the film surface. The photoelectrons more easily spill out of the bulk into the vacuum under such an electric field, resulting in the low IP and V_{OC}. With increasing thickness, the SQ molecules in the films no longer retain the oriented structure, leading to randomization of the aligned dipole moments and disappearance of the electric fields at the D/A interface. Consequently, up-shifted IP and V_{OC} are obtained. On the basis of our findings, we believe that V_{OC} in OPV cells greatly depends on the molecular orientation at the D/A interface, where the interfacial dipole moment plays an important role. V_{OC} can be tuned/optimized by governing the strength (density) and direction of the interfacial dipole moment. It can be briefly concluded that the origin of the thickness-dependent V_{OC} is caused by (1) recombination at the anode, which impacts the energy loss, (2) recombination at the D/A interface determined by interfacial disorder, which influences the strength of electronic coupling, and (3) the shifted IP induced by variations in the molecular orientation, which affects the direction and strength of the interfacial dipole moment. Introduction of the BP2T buffer layer is effective in enhancing V_{OC} because of the suppressed recombination at the anode surface; however, it has less effect in altering the molecular orientation of the SQ films. Although V_{OC} has been successfully raised to 0.86 V, the cell efficiency decreases because of the reduction in J_{SC} and FF. Further improvement in V_{OC} without sacrificing J_{SC} and FF can be realized by developing SQ films with standing-up molecular orientation (nitrogen-terminated ends exposed to the vacuum).

CONCLUSIONS

We have investigated the influence of the device structure on V_{OC} in SQ/C_{60} bilayer cells. By simple adjustment of the SQ thickness from 6 to 40 nm, V_{OC} shifts 40% from 0.62 to 0.86 V. Discontinuous SQ films at low thicknesses result in a Schottky contact between ITO and C_{60}, which sparks low V_{OC} values. When ITO substrates are covered with a thin layer of BP2T, V_{OC} has obviously been improved because of the reduced surface recombination. Variation in the IP of SQ films with different thicknesses is found to be another crucial reason for the shifts in V_{OC}. In spite of the amorphous nature, the SQ molecules are found to be lying-down on the substrates with noncentrosymmetric orientation at low thicknesses while gradually changing into a random structure as the film thicknesses increase. The orientation-dependent electronic coupling that influences recombination at the D/A interface may also result in variations in V_{OC}. DFT calculations suggest that aligned dipole moments at the D/A interface would be generated with an oriented structure at low thicknesses, rendering an electric field pointing from donor to acceptor, which leads to low IP and V_{OC}. As the film thickness increases, the SQ films evolve into a random structure, causing decreases in the strength (density) and randomization in the direction of the dipole moments, which accounts for the up-shifted IP and V_{OC}. Our findings suggest that optimization of the cell performance for high V_{OC} must involve not only tailoring the energy levels of the organic molecules but also governing the molecular orientation at the D/A interface to achieve reduced electronic coupling and suitable interfacial dipole alignment.

ASSOCIATED CONTENT

Supporting Information

Additional data including substrate morphology, energy alignment, temperature-dependent dark current, GIWAXS, DFT-calculated FTIR spectrum, Gaussian-fitted FTIR spectra, and movies illustrating vibration modes. The Supporting Information is available free of charge on the ACS Publications website at DOI: 10.1021/acsami.5b01723.

AUTHOR INFORMATION

Corresponding Author

*E-mail: wang-zhiping@aist.go.jp.

Notes

The authors declare no competing financial interest.

ACKNOWLEDGMENTS

This work was financially supported by the program from the Japan New Energy and Industrial Technology Development Organization. The synchrotron radiation experiments were performed at the BL46XU of SPring-8 with the approval of the Japan Synchrotron Radiation Research Institute (Proposals 2014A1507 and 2014B1614).

REFERENCES

(1) Su, Y. W.; Lan, S. C.; Wei, K. H. Organic Photovoltaics. *Mater. Today* **2012**, *15*, 554−562.

DOI: 10.1021/acsami.5b01723
ACS Appl. Mater. Interfaces 2015, 7, 10814−10822

(2) Li, G.; Zhu, R.; Yang, Y. Polymer Solar cells. *Nat. Photonics* **2012**, *6*, 153−161.
(3) Kumar, P.; Chand, S. Recent Progress and Future Aspects of Organic Solar Cells. *Prog. Photovoltaics* **2012**, *20*, 377−415.
(4) Xiao, Z.; Yuan, Y.; Yang, B.; VanDerslice, J.; Chen, J.; Dyck, O.; Duscher, G.; Huang, J. Universal Formation of Compositionally Graded Bulk Heterojunction for Efficiency Enhancement in Organic Photovoltaics. *Adv. Mater.* **2014**, *26*, 3068−3075.
(5) Mazzio, K. A.; Luscombe, C. K. The Future of Organic Photovoltaics. *Chem. Rev. Soc.* **2015**, *44*, 78−90.
(6) Kyaw, A. K. K.; Wang, D. H.; Wynands, D.; Zhang, J.; Nguyen, T.-Q.; Bazan, G. C.; Heeger, A. J. Improved Light Harvesting and Improved Efficiency by Insertion of an Optical Spacer (ZnO) in Solution-Processed Small-Molecule Solar Cells. *Nano Lett.* **2013**, *13*, 3796−3801.
(7) He, Z. C.; Zhong, C. M.; Su, S. J.; Xu, M.; Wu, H. B.; Cao, Y. Enhanced Power-Conversion Efficiency in Polymer Solar Cells using an Inverted Device Structure. *Nat. Photonics* **2012**, *6*, 591−595.
(8) Che, X.; Xiao, X.; Zimmerman, J. D.; Fan, D.; Forrest, S. R. High-Efficiency, Vacuum-Deposited, Small-Molecule Organic Tandem and Triple-Junction Photovoltaic Cells. *Adv. Energy Mater.* **2014**, *4*, 1400568.
(9) Chen, C.-C.; Chang, W.-H.; Yoshimura, K.; Ohya, K.; You, J.; Gao, J.; Hong, Z.; Yang, Y. An Efficient Triple-Junction Polymer Solar Cell Having a Power Conversion Efficiency Exceeding 11%. *Adv. Mater.* **2014**, *26*, 5670−5677.
(10) Mishra, A.; Bäuerle, P. Small Molecule Organic Semiconductors on the Move: Promises for Future Solar Energy Technology. *Angew. Chem., Int. Ed.* **2012**, *51*, 2020−2067.
(11) Schober, M.; Anderson, M.; Thomschke, M.; Widmer, J.; Furno, M.; Scholz, R.; Lüssem, B.; Leo, K. Quantitative Description of Charge-Carrier Transport in a White Organic Light-Emitting Diode. *Phys. Rev. B* **2011**, *84*, 165326.
(12) Zhou, Y.; Taima, T.; Miyadera, T.; Yamanari, T.; Kitamura, M.; Nakatsu, K.; Yoshida, Y. Glancing Angle Deposition of Copper Iodide Nanocrystals for Efficient Organic Photovoltaics. *Nano Lett.* **2012**, *12*, 4146−4152.
(13) Zhou, Y.; Taima, T.; Kuwabara, T.; Takahashi, K. Efficient Small-Molecule Photovoltaic Cells Using a Crystalline Diindenoperylene Film as a Nanostructured Template. *Adv. Mater.* **2013**, *25*, 6069−6075.
(14) Wang, Z.-P.; Miyadera, T.; Yamanari, T.; Yoshida, Y. Templating Effects in Molecular Growth of Blended Films for Efficient Small-Molecule Photovoltaics. *ACS Appl. Mater. Interfaces* **2014**, *6*, 6369−6377.
(15) Wang, Z.; Miyadera, T.; Saeki, A.; Zhou, Y.; Seki, S.; Shibata, Y.; Yamanari, T.; Matsubara, K.; Yoshida, Y. Structural Influences on Charge Carrier Dynamics for Small-Molecule Organic Photovoltaics. *J. Appl. Phys.* **2014**, *116*, 013105.
(16) Scharber, M. C.; Mühlbacher, D.; Koppe, M.; Denk, P.; Waldauf, C.; Heeger, A. J.; Brabec, C. J. Design Rules for Donors in Bulk-Heterojunction Solar Cells—Towards 10% Energy-Conversion Efficiency. *Adv. Mater.* **2006**, *18*, 789−794.
(17) Rand, B.; Burk, D.; Forrest, S. Offset Energies at Organic Semiconductor Heterojunctions and Their Influence on the Open-Circuit Voltage of Thin-Film Solar Cells. *Phys. Rev. B* **2007**, *75*, 115327.
(18) Maurano, A.; Hamilton, R.; Shuttle, C. G.; Ballantyne, A. M.; Nelson, J.; O'Regan, B.; Zhang, W.; McCulloch, I.; Azimi, H.; Morana, M.; Brabec, C. J.; Durrant, J. R. Recombination Dynamics as a Key Determinant of Open Circuit Voltage in Organic Bulk Heterojunction Solar Cells: A Comparison of Four Different Donor Polymers. *Adv. Mater.* **2010**, *22*, 4987−4992.
(19) Zhong, Y.; Tada, A.; Izawa, S.; Hashimoto, K.; Tajima, K. Enhancement of V_{OC} without Loss of J_{SC} in Organic Solar Cells by Modification of Donor/Acceptor Interfaces. *Adv. Energy Mater.* **2014**, *4*, 1301332.
(20) Zimmerman, J. D.; Lassiter, B. E.; Xiao, X.; Sun, K.; Dolocan, A.; Gearba, R.; Vanden Bout, D. A.; Stevenson, K. J.; Wickramasinghe, P.; Thompson, M. E.; Forrest, S. R. Control of Interface Order by Inverse Quasi-Epitaxial Growth of Squaraine/Fullerene Thin Film Photovoltaics. *ACS Nano* **2013**, *7*, 9268−9275.
(21) Song, B.; Rolin, C.; Zimmerman, J. D.; Forrest, S. R. Effect of Mixed Layer Crystallinity on the Performance of Mixed Heterojunction Organic Photovoltaic Cells. *Adv. Mater.* **2014**, *26*, 2914−2918.
(22) Liu, Z.; Ju, H.; Lee, E.-C. Improvement of Polycarbazole-Based Organic Bulk-Heterojunction Solar Cells Using 1,8-Diiodooctane. *Appl. Phys. Lett.* **2013**, *103*, 133308.
(23) Lu, L.; Yu, L. Understanding Low Bandgap Polymer PTB7 and Optimizing Polymer Solar Cells Based on It. *Adv. Mater.* **2014**, *26*, 4413−4430.
(24) Wang, M.; Wang, H.; Yokoyama, T.; Liu, X.; Huang, Y.; Zhang, Y.; Nguyen, T.-Q.; Aramaki, S.; Bazan, G. C. High Open Circuit Voltage in Regioregular Narrow Band Gap Polymer Solar Cells. *J. Am. Chem. Soc.* **2014**, *136*, 12576−12579.
(25) Liu, J.; Shi, Y. J.; Yang, Y. Solvation-Induced Morphology Effects on the Performance of Polymer-Based Photovoltaic Devices. *Adv. Funct. Mater.* **2001**, *11*, 420−424.
(26) Qi, B.; Zhang, Z.-G.; Wang, J. Uncovering the Role of Cathode Buffer Layer in Organic Solar Cells. *Sci. Rep.* **2014**, *5*, 7803.
(27) Piersimoni, F.; Chambon, S.; Vandewal, K.; Mens, R.; Boonen, T.; Gadisa, A.; Izquierdo, M.; Filippone, S.; Ruttens, B.; D'Haen, J.; Martin, N.; Lutsen, L.; Vanderzande, D.; Adriaensens, P.; Manca, J. V. Influence of Fullerene Ordering on the Energy of the Charge-Transfer State and Open-Circuit Voltage in Polymer:Fullerene Solar Cells. *J. Phys. Chem. C* **2011**, *115*, 10873−10880.
(28) Opitz, A.; Bronner, M.; Brütting, W.; Himmerlich, M.; Schaefer, J. A.; Krischok, S. Electronic Properties of Organic Semiconductor Blends: Ambipolar Mixtures of Phthalocyanine and Fullerene. *Appl. Phys. Lett.* **2007**, *90*, 212112.
(29) Ryan, J. W.; Kirchartz, T.; Viterisi, A.; Nelson, J.; Palomares, E. Understanding the Effect of Donor Layer Thickness and a MoO_3 Hole Transport Layer on the Open-Circuit Voltage in Squaraine/C_{60} Bilayer Solar Cells. *J. Phys. Chem. C* **2013**, *117*, 19866−19874.
(30) Kinoshita, Y.; Takenaka, R.; Murata, H. Independent Control of Open-Circuit Voltage of Organic Solar Cells by Changing Film Thickness of MoO_3 Buffer Layer. *Appl. Phys. Lett.* **2008**, *92*, 243309.
(31) Tress, W.; Leo, K.; Riede, M. Influence of Hole-Transport Layers and Donor Materials on Open-Circuit Voltage and Shape of *I*−*V* Curves of Organic Solar Cells. *Adv. Funct. Mater.* **2011**, *21*, 2140−2149.
(32) Zeng, L.; Tang, C. W.; Chen, S. H. Effects of Active Layer Thickness and Thermal Annealing on Polythiophene: Fullerene Bulk Heterojunction Photovoltaic Devices. *Appl. Phys. Lett.* **2010**, *97*, 053305.
(33) Sun, K.; Xiao, Z.; Lu, S.; Zajaczkowski, W.; Pisula, W.; Hanssen, E.; White, J. M.; Williamson, R. M.; Subbiah, J.; Ouyang, J.; Holmes, A. B.; Wong, W. W. H.; Jones, D. J. A Molecular Nematic Liquid Crystalline Material for High-Performance Organic Photovoltaics. *Nat. Commun.* **2015**, *6*, 6013.
(34) Murphy, L.; Hong, W.; Aziz, H.; Li, Y. Organic Photovoltaics with Thick Active Layers (~800 nm) using a High Mobility Polymer Donor. *Sol. Energy Mater. Sol. Cells* **2013**, *114*, 71−81.
(35) Yan, S.; Yang, Y. Efficient Organic Heterojunction Photovoltaic Cells Based on Triplet Materials. *Adv. Mater.* **2005**, *17*, 2841−2844.
(36) Sievers, D. W.; Shrotriya, V.; Yang, Y. J. Modeling Optical Effects and Thickness Dependent Current in Polymer Bulk-Heterojunction Solar Cells. *Appl. Phys. Lett.* **2006**, *100*, 114509.
(37) Credgington, D.; Hamilton, R.; Atienzar, P.; Nelson, J.; Durrant, J. R. Non-Geminate Recombination as the Primary Determinant of Open-Circuit Voltage in Polythiophene:Fullerene Blend Solar Cells: An Analysis of the Influence of Device Processing Conditions. *Adv. Funct. Mater.* **2011**, *21*, 2744−2753.
(38) Anger, F.; Glowatzki, H.; Franco-Cañellas, A.; Bürker, C.; Gerlach, A.; Scholz, R.; Sakamoto, Y.; Suzuki, T.; Koch, N.; Schreiber, F. Interface Dipole and Growth Mode of Partially and Fully

DOI: 10.1021/acsami.5b01723
ACS Appl. Mater. Interfaces 2015, 7, 10814−10822

Fluorinated Rubrene on Au(111) and Ag(111). *J. Phys. Chem. C* **2015**, *119*, 6769−6776.
(39) Krause, S.; Casu, M. B.; Schöll, A.; Umbach, E. Determination of Transport Levels of Organic Semiconductors by UPS and IPS. *New J. Phys.* **2008**, *10*, 085001.
(40) Sinha, S.; Mukherjee, M. Thickness Dependent Electronic Structure and Morphology of Rubrene Thin Films on Metal, Semiconductor, and Dielectric Substrates. *J. Appl. Phys.* **2013**, *114*, 083709.
(41) Zimmerman, J. D.; Xiao, X.; Renshaw, C. K.; Wang, S.; Diev, V. V.; Thompson, M. E.; Forrest, S. R. Independent Control of Bulk and Interfacial Morphologies of Small Molecular Weight Organic Heterojunction Solar Cells. *Nano Lett.* **2012**, *12*, 4366−4371.
(42) Fu, Y.-T.; da Silva Filho, D. A.; Sini, G.; Asiri, A. M.; Aziz, S. G.; Risko, C.; Brédas, J.-L. Structure and Disorder in Squaraine−C_{60} Organic Solar Cells: A Theoretical Description of Molecular Packing and Electronic Coupling at the Donor-Acceptor Interface. *Adv. Funct. Mater.* **2014**, *24*, 3790−3798.
(43) Duhm, S.; Heimel, G.; Salzmann, I.; Glowatzki, H.; Johnson, R. L.; Vollmer, A.; Rabe, J.; Koch, H. Orientation-Dependent Ionization Energies and Interface Dipoles in Ordered Molecular Assemblies. *Nat. Mater.* **2008**, *7*, 326−332.
(44) Tada, A.; Geng, Y.; Wei, Q.; Hashimoto, K.; Tajima, K. Tailoring Organic Heterojunction Interfaces in Bilayer Polymer Photovoltaic Devices. *Nat. Mater.* **2011**, *10*, 450−455.
(45) Chen, G.; Yokoyama, D.; Sasabe, H.; Hong, Z.; Yang, Y.; Kido, J. Optical and Electrical Properties of a Squaraine Dye in Photovoltaic Cells. *Appl. Phys. Lett.* **2012**, *101*, 083904.
(46) Wang, S.; Mayo, E. I.; Perez, M. D.; Griffe, L.; Wei, G.; Djurovich, P. I.; Forrest, S. R.; Thompson, M. E. High Efficiency Organic Photovoltaic Cells Based on a Vapor Deposited Squaraine Donor. *Appl. Phys. Lett.* **2009**, *94*, 233304.
(47) Boix, P. P.; Wienk, M. M.; Janssen, R. A. J.; Garcia-Belmonte, G. Open-Circuit Voltage Limitation in Low-Bandgap Diketopyrrolopyrrole-Based Polymer Solar Cells Processed from Different Solvents. *J. Phys. Chem. C* **2011**, *115*, 15075−15080.
(48) Cheyns, D.; Poortmans, J.; Heremans, P. Analytical Model for the Open-Circuit Voltage and Its Associated Resistance in Organic Planar Heterojunction Solar Cells. *Phys. Rev. B* **2008**, *77*, 165332.
(49) Hörmann, U.; Lorch, C.; Hinderhofer, A.; Gerlach, A.; Gruber, M.; Kraus, J.; Sykora, B.; Grob, S.; Linderl, T.; Wilke, A.; Opitz, A.; Hansson, R.; Anselmo, A. S.; Ozawa, Y.; Nakayama, Y.; Ishii, H.; Koch, N.; Moons, E.; Schreiber, F.; Brütting, W. V_{OC} from a Morphology Point of View: the Influence of Molecular Orientation on the Open Circuit Voltage of Organic Planar Heterojunction Solar Cells. *J. Phys. Chem. C* **2014**, *118*, 26462−26470.
(50) Cowan, S. R.; Roy, A.; Heeger, A. J. Recombination in Polymer−Fullerene Bulk Heterojunction Solar Cells. *Phys. Rev. B* **2010**, *82*, 245207.
(51) Vandewal, K.; Tvingstedt, K.; Gadisa, A.; Inganas, O.; Manca, J. V. Relating the Open-Circuit Voltage to Interface Molecular Properties of Donor:Acceptor Bulk Heterojunction Solar Cells. *Phys. Rev. B* **2010**, *81*, 125204.
(52) Potscavage, W. J.; Yoo, S.; Kippelen, B. Origin of the Open-Circuit Voltage in Multilayer Heterojunction Organic Solar Cells. *Appl. Phys. Lett.* **2008**, *93*, 193308.
(53) Widmer, J.; Tietze, M.; Leo, K.; Riede, M. Open-Circuit Voltage and Effective Gap of Organic Solar Cells. *Adv. Funct. Mater.* **2013**, *23*, 5814−5821.
(54) Chirvase, D.; Chiguvare, Z.; Knipper, M.; Parisi, J.; Dyakonov, V.; Hummelen, J. C. Temperature Dependent Characteristics of Poly(3 Hexylthiophene)−Fullerene Based Heterojunction Organic Solar Cells. *J. Appl. Phys.* **2003**, *93*, 3376−3383.
(55) Dyakonov, V. Mechanisms Controlling the Efficiency of Polymer Solar Cells. *Appl. Phys. A: Mater. Sci. Process.* **2004**, *79*, 21−25.
(56) Mauer, R.; Howard, I. A.; Laquai, F. Effect of Nongeminate Recombination on Fill Factor in Polythiophene/Methanofullerene Organic Solar Cells. *J. Phys. Chem. Lett.* **2010**, *1*, 3500−3505.
(57) Mikhnenko, O. V.; Cordella, F.; Sieval, A. B.; Hummelen, J. C.; Blom, P. W. M.; Loi, M. A. Temperature Dependence of Exciton Diffusion in Conjugated Polymers. *J. Phys. Chem. B* **2008**, *112*, 11601−11604.
(58) Shen, Y. L.; Klein, M. W.; Jacobs, D. B.; Scott, J. C.; Malliaras, G. G. Mobility-Dependent Charge Injection into an Organic Semiconductor. *Phys. Rev. Lett.* **2001**, *86*, 3867−3870.
(59) Kirchartz, T.; Deledalle, F.; Tuladhar, P. S.; Durrant, J. R.; Nelson, J. On the Differences between Dark and Light Ideality Factor in Polymer:Fullerene Solar Cells. *J. Phys. Chem. Lett.* **2013**, *4*, 2371−2376.
(60) Kirchartz, T.; Nelson, J. Meaning of Reaction Orders in Polymer:Fullerene Solar Cells. *Phys. Rev. B* **2012**, *86*, 165201.
(61) Smoluchowski, R. Anisotropy of the Electronic Work Function of Metals. *Phys. Rev.* **1941**, *60*, 661−674.
(62) Lang, N. D.; Kohn, W. Theory of Metal Surfaces: Work Function. *Phys. Rev. B* **1971**, *3*, 1215−1223.
(63) Friedlein, R.; Crispin, X.; Pickholz, M.; Keil, M.; Stafström, S.; Salaneck, W. R. High Intercalation Levels in Lithium Perylene Stoichiometric Compounds. *Chem. Phys. Lett.* **2002**, *354*, 389−394.
(64) Ivanco, J.; Winter, B.; Netzer, T. R.; Ramsey, M. G. Substrate-Mediated Electronic Structure and Properties of Sexiphenyl Films. *Adv. Mater.* **2003**, *15*, 1812−1815.
(65) Fukagawa, H.; Yamane, H.; Kataoka, T.; Kera, S.; Nakamura, M.; Kudo, K.; Ueno, N. Origin of the Highest Occupied Band Position in Pentacene Films from Ultraviolet Photoelectron Spectroscopy: Hole Stabilization versus Band Dispersion. *Phys. Rev. B* **2006**, *73*, 245310.
(66) Ivanco, J.; Netzer, F. P.; Ramsey, M. G. On Validity of the Schottky−Mott Rule in Organic Semiconductors: Sexithiophene On Various Substrates. *J. Appl. Phys.* **2007**, *101*, 103712.
(67) Wei, G.; Wang, S.; Renshaw, K.; Thompson, M. E.; Forrest, S. R. Solution-Processed Squaraine Bulk Heterojunction Photovoltaic Cells. *ACS Nano* **2010**, *4*, 1927−1934.
(68) Hasegawa, Y.; Matsumoto, L.; Kitamura, S.; Amino, S.; Katada, S.-I.; Nishijo, J. Optimum Condition of Fourier Transform Infrared Multiple-Angle Incidence Resolution Spectrometry for Surface Analysis. *Anal. Chem.* **2002**, *74*, 6049−6054.
(69) Hasegawa, T. Analysis of Structurally Heterogeneous Langmuir−Blodgett Films of Folded/Unfolded Long-Chain Molecules by Infrared Multiple-Angle Incidence Resolution Spectroscopy. *Anal. Chem.* **2006**, *78*, 6121−6125.
(70) Spencer, S. D.; Bougher, C.; Heaphy, P. J.; Murcia, V. M.; Gallivan, C. P.; Monfette, A.; Andersen, J. D.; Cody, J. A.; Conrad, B. R.; Collison, C. J. The Effect of Controllable Thin Film Crystal Growth on the Aggregation of a Novel High Panchromaticity Squaraine Viable for Organic Solar Cells. *Sol. Energy Mater. Sol. Cells* **2013**, *112*, 202−208.
(71) Chen, G.; Sasabe, H.; Sasaki, Y.; Katagiri, H.; Wang, X.-F.; Sano, T.; Hong, Z.; Yang, Y.; Kido, J. A Series of Squaraine Dyes: Effects of Side Chain and the Number of Hydroxyl Groups on Material Properties and Photovoltaic Performance. *Chem. Mater.* **2014**, *26*, 1356−1364.

DOI: 10.1021/acsami.5b01723
ACS Appl. Mater. Interfaces 2015, 7, 10814−10822